



Contents lists available at ScienceDirect

Journal of Quantitative Spectroscopy & Radiative Transfer

journal homepage: www.elsevier.com/locate/jqsrt

The ACE-FTS atlas of the infrared solar spectrum

Frank Hase^{a,*}, Lloyd Wallace^b, Sean D. McLeod^c, Jeremy J. Harrison^d, Peter F. Bernath^d

^a Institut für Meteorologie und Klimaforschung, Forschungszentrum Karlsruhe, Postfach 3640, D-76021 Karlsruhe, Germany

^b Kitt Peak National Observatory, National Optical Astronomy Observatories, Tucson, AZ, 85726 USA

^c Department of Chemistry, University of Waterloo, Waterloo, ON, Canada N2L 3G1

^d Department of Chemistry, University of York, Heslington, York, YO10 5DD UK

ARTICLE INFO

Article history:

Received 25 August 2009

Received in revised form

22 October 2009

Accepted 23 October 2009

Keywords:

Infrared spectroscopy

Solar spectrum

Solar lines

ABSTRACT

The ACE-FTS is a space-borne Fourier transform spectrometer onboard SCISAT-1. The satellite was launched in August 2003 and since February 2004 the ACE-FTS has been performing solar occultation measurements in order to infer the chemical composition of the terrestrial atmosphere. The individual spectra recorded at the highest limb tangent altitudes (above 160 km) are by definition “high sun” spectra and contain no atmospheric contribution. In this work, an empirical solar spectrum covering the 700 to 4430 cm⁻¹ spectral range has been constructed from an average of 224,782 individual ACE-FTS solar spectra. Line assignments have been made for about 12,000 lines. The spectrum and two line lists are provided in the supplemental material attached to this work. Due to the excellent noise level achieved in the ACE-FTS solar atlas presented here, numerous weak absorption features are assigned which were not detectable in the ATMOS solar observations.

© 2009 Elsevier Ltd. All rights reserved.

1. Introduction

The infrared solar spectrum can be studied from the ground in atmospheric window regions, but even in these window regions the recorded “solar” spectrum is heavily contaminated by telluric absorption lines. Aircraft- and balloon-borne spectrometers allow measurements at a significantly lower air mass, extending the observations into spectral regions inaccessible from ground, but still suffer from significant telluric interference. Only satellite-borne spectrometers allow a pure solar spectrum to be recorded over the entire infrared spectral region. The spectra collected by the ATMOS (Atmospheric Trace Molecule Spectroscopy) Fourier transform spectrometer (FTS) during four Space Shuttle missions (Spacelab 3, ATLAS 1–3) are an invaluable source for the study of the infrared solar spectrum. The original ATMOS atlas of the infrared spectrum of the sun was

compiled from 4800 Spacelab 3 solar spectra [1] and about 2500 solar lines were assigned [2]. A more recent ATMOS solar atlas is also available (in pieces due to the spectral filters used) based on 40,000 spectra from the ATLAS-3 mission [3].

Like ATMOS, the ACE-FTS onboard the Canadian SCISAT-1 satellite performs solar occultation measurements to infer the chemical composition of the terrestrial atmosphere. SCISAT-1 satellite was launched by NASA in August 2003 and the ACE-FTS has been taking spectra since February 2004 [4]. The spectral resolution of the ACE-FTS is a factor of 2 less than ATMOS, the spectral coverage is similar, but much higher signal-to-noise ratios can be achieved for the solar spectrum due to the large number of available ACE spectra. Moreover, ATMOS used a photoconductive HgCdTe detector in the longwave spectral bands 1 and 2 [5], whereas the ACE-FTS uses a photovoltaic HgCdTe detector, which gives an improved zero baseline because of the smaller detector nonlinearity. The spectra recorded by the ACE-FTS are a unique dataset that complement and extend the ATMOS measurements.

This work is structured in the following manner: Section 2 gives a summary of the ACE-FTS, Section 3

* Corresponding author. Tel.: +49 7247 82 2434;

fax: +49 7247 82 4742.

E-mail address: frank.hase@imk.fzk.de (F. Hase).

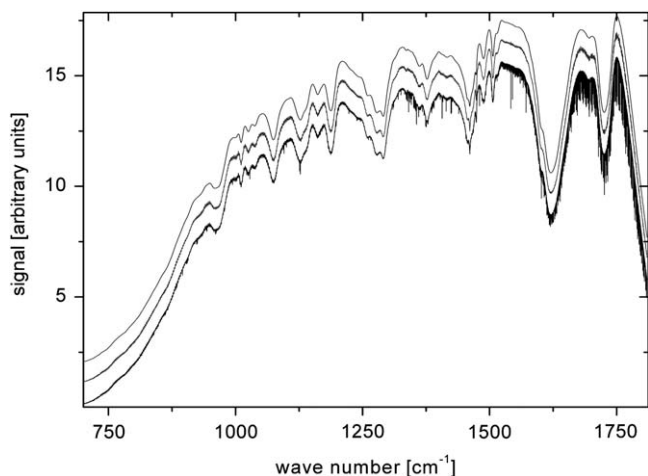


Fig. 1. Bottom curve: averaged raw ACE-FTS spectrum recorded by the HgCdTe detector, 224,782 individual spectra recorded from February 2004 to January 2008 were used. A Norton–Beer strong apodization function has been applied. Middle curve (ordinate offset applied for readability): the ACE spectrum divided by the modelled solar transmission. All prominent solar features are removed. Upper curve (ordinate offset applied for readability): the spectrally smooth empirical response curve.

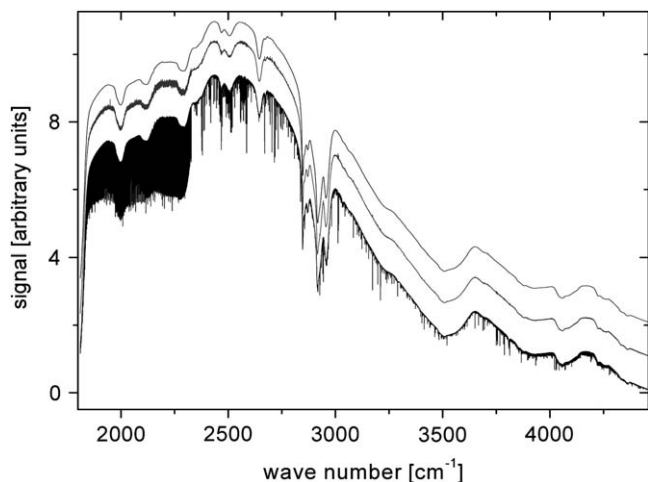


Fig. 2. Bottom curve: averaged raw ACE-FTS spectrum recorded by the InSb detector, 224,782 individual spectra recorded in the time frame from February 2004 to January 2008 were used. A Norton–Beer strong apodization function has been applied. Middle curve (ordinate offset applied for readability): the ACE spectrum divided by the modelled solar transmission. All prominent solar features are removed. Upper curve (ordinate offset applied for readability): the spectrally smooth empirical response curve.

explains how the solar transmittance spectrum has been constructed from the raw spectra, and the final Section 4 gives a description of the ACE-FTS solar line lists and introduces the ACE-FTS solar atlas which has been generated from the solar transmittance spectrum.

2. Description of the ACE-FTS spectra

SCISAT-1 or the Atmospheric Chemistry Experiment (ACE) is a Canadian satellite designed to measure a large number of atmospheric constituents using the technique of solar occultation [4]. The original primary mission goal was to study stratospheric ozone chemistry in the Arctic, but ACE has made a wide range of additional observations

of, for example, organic molecules in the troposphere and of polar mesospheric clouds (see <http://www.ace.uwaterloo.ca/> for more information). SCISAT-1 was launched by NASA into a circular orbit at an altitude of 650 km and an inclination angle of 74° on August 12, 2003. Although ACE had a nominal 2 year mission, it has functioned successfully for more than six years with only minor problems.

The primary ACE instrument is a high resolution Fourier transform spectrometer (ACE-FTS) that covers the $2\text{--}13\ \mu\text{m}$ range ($750\text{--}4400\ \text{cm}^{-1}$) at $0.02\ \text{cm}^{-1}$ unapodized spectral resolution. The ACE-FTS is a double-passed cubecorner Michelson interferometer with a maximum optical path difference of 25 cm that was built by ABB-Bomem in Quebec City. The FTS uses two photovoltaic detectors (InSb and HgCdTe), aligned with

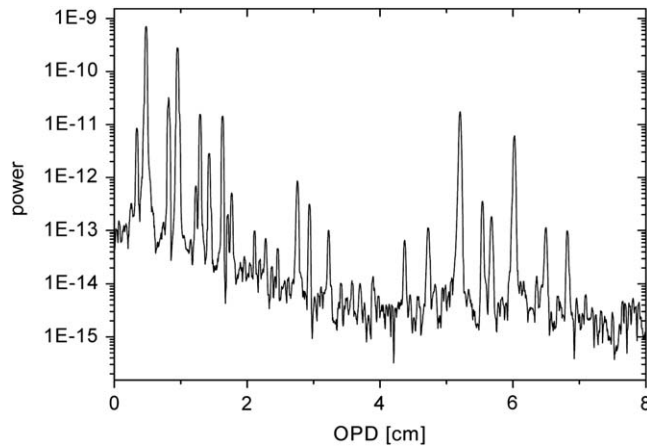


Fig. 3. Power spectrum showing distinct channelling frequencies. This spectrum is calculated by the Fourier transform of the ratio of the ACE HgCdTe spectrum after removal of the modelled solar lines, divided by the empirical response curve. The power in the leading spikes exceeds the noise level by several orders of magnitude.

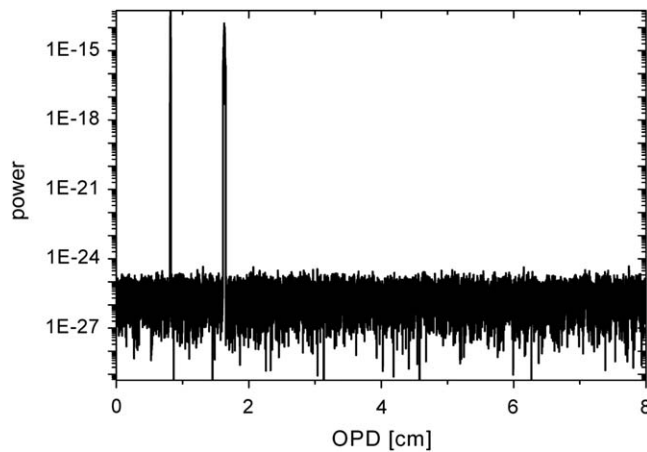


Fig. 4. Power spectrum showing distinct channelling frequencies for the InSb spectrum. The power in the leading spikes exceeds the noise level by several orders of magnitude.

Table 1

Frequency ranges taken into account for removal of HgCdTe channel fringes. (As the spectral axis bears the unit cm^{-1} , the frequency unit of the fringe modulation is given in cm.)

HgCdTe bandpass #	Frequency range (cm)
1	0.32–0.36
2	0.42–0.52
3	0.79–0.84
4	0.92–1.00
5	1.18–1.32
6	1.40–1.47
7	1.61–1.65
8	1.75–1.786
9	2.69–2.78
10	2.92–2.95
11	5.07–5.25
12	5.51–5.57
13	5.89–6.06
14	6.46–6.52
15	6.80–6.85

Table 2

Frequency ranges taken into account for removal of InSb channel fringes. (As the spectral axis bears the unit cm^{-1} , the frequency unit of the fringe modulation is given in cm.)

InSb bandpass #	Frequency range (cm)
1	0.81–0.825
2	1.61–1.65

a dichroic element (splitting at 1810cm^{-1}) to have the same field of view. A suntracker mirror points to the nominal center of radiance of the sun and the external field of view is 1.25 mrad compared to the sun diameter of 9 mrad.

The spectral resolution of ACE is a factor of 2 less than ATMOS (0.01cm^{-1} for a 50 cm maximum optical path difference), but this has only a small (but not negligible) effect on the observed solar spectrum because most of the

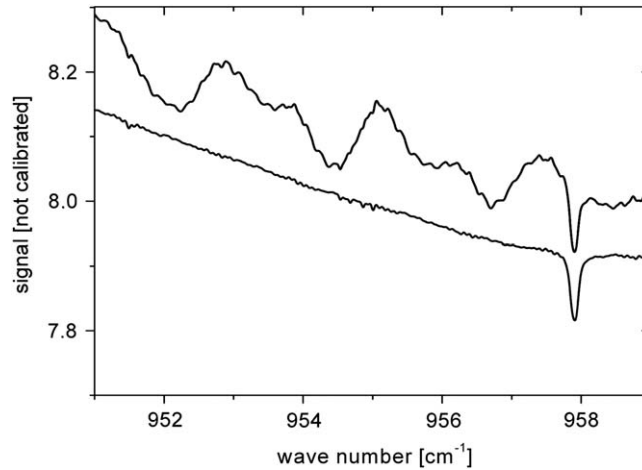


Fig. 5. Section of the ACE-FTS HgCdTe spectrum before and after removing the channel fringes. Much weaker solar lines can be discerned after the correction.

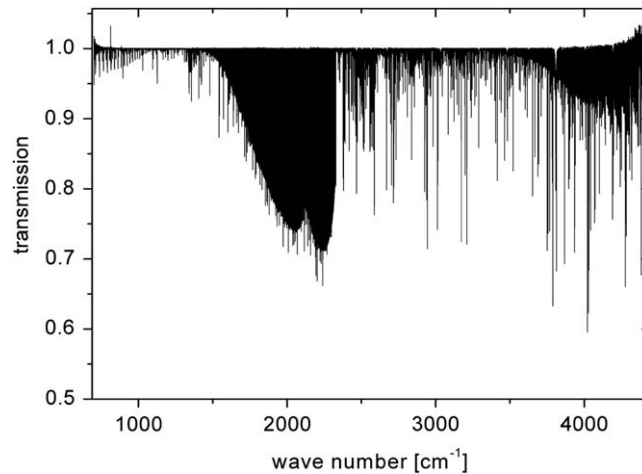


Fig. 6. The final ACE-FTS solar transmission spectrum. The apparent bending of the continuum level near the low and high wavenumber ends is actually due to the envelope of increasing noise; the continuum level is unity over the whole region.

solar lines are wider than 0.02 cm^{-1} . The nominal total range ($650\text{--}4800 \text{ cm}^{-1}$) of the ATMOS measurements is also wider than for ACE, but the ATMOS range was divided into pieces by the use of filters and the signal-to-noise ratio in any piece was typically 100 for a single scan. For ACE the entire spectral range was covered in each scan and the signal-to-noise ratio for a single 2 s scan is more than 300 over most of the spectral range. Another important difference between ACE and ATMOS is that ATMOS data were contaminated by CO_2 and H_2O lines from residual gas in the spectrometer tank.

In normal operation the ACE-FTS typically records a sequence of about 70 spectra for each sunrise or sunset. Each ACE occultation consists of three types of observations: 16 spectra of deep space used to correct for instrument self emission, 16 high sun spectra with tangent heights above 160 km used as a reference and about 40–60 atmospheric spectra with tangent heights

between 5 and 150 km (depending on orbit geometry). It is these 16 high sun spectra that are used to make the ACE solar atlas. Unfortunately the high sun spectra suffer from the presence of channel fringes that need to be corrected. This channelling is not a problem for normal atmospheric transmission data because the atmospheric spectra are divided by the high sun spectra, which cancels the channel fringes almost completely.

3. Construction of a mean ACE-FTS solar transmission spectrum

In the first step, a mean raw solar spectrum has been constructed by averaging 224,782 individual ACE-FTS spectra, observed at tangent altitudes above 160 km. Due to the orbital motions of both the spacecraft and the Earth, simple co-adding of all the spectra is not

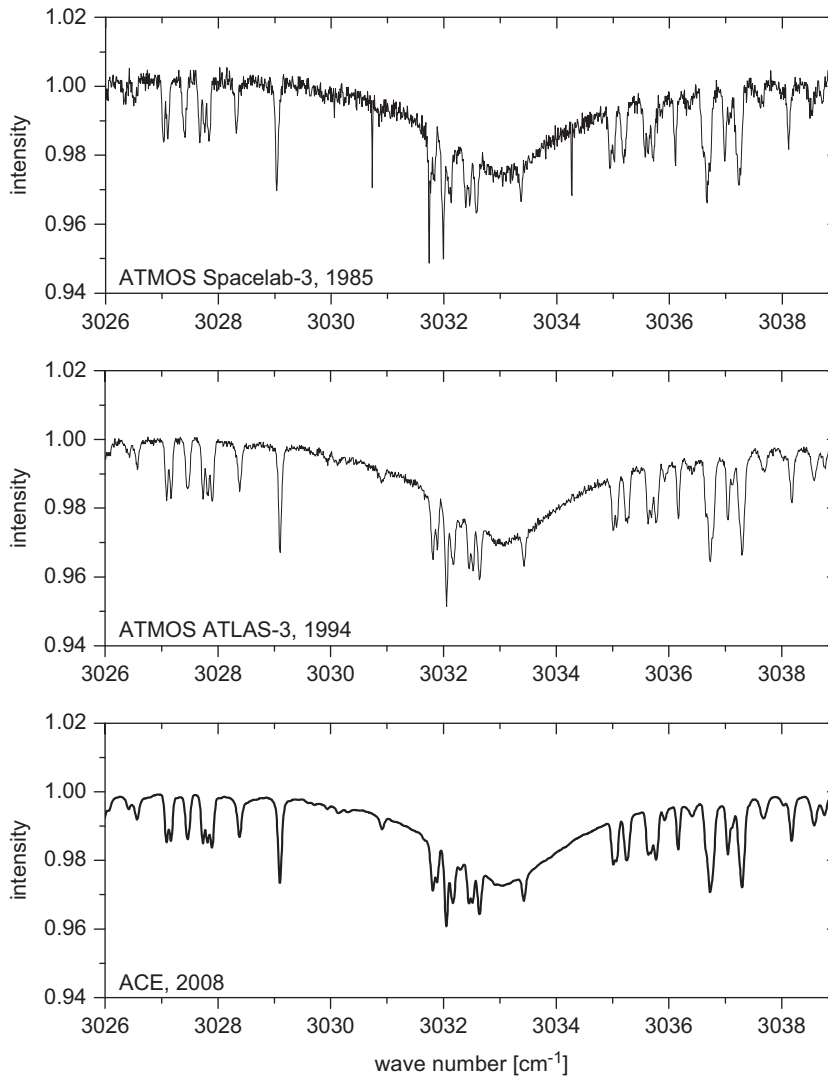


Fig. 7. A comparison of the ACE solar transmission spectrum and the two ATMOS results.

possible, as the spectral abscissa is stretched by an individual Doppler scaling factor. Instead, orbit modelling software is used to calculate the relative velocity between the spacecraft and the sun to perform an initial wave-number calibration. Then, orbit-to-orbit variations in the FTS metrology laser temperature are corrected by fitting high-altitude (80–100 km) reference CO₂ lines in atmospheric spectra from the corresponding occultation.

The averaged raw spectra are shown in Figs. 1 and 2 for the spectral regions covered by the HgCdTe and InSb detectors, respectively. A Norton–Beer strong apodization function has been applied to suppress any ringing around lines which are not fully resolved. Over nearly the entire spectral domain covered by the ACE-FTS channel fringes are larger than the noise level, so it is essential to characterise and to remove these artefacts. To achieve this goal, the following procedure has been applied: a predicted solar spectrum was calculated using the line-by-line model

developed by Hase et al. [6]. This model merges ATMOS, ground- and balloon-borne FTS measurements with theoretical modelling of the solar spectrum and is assumed to present the prior best knowledge of solar spectral features in the mid-IR (not taking into account ACE-FTS spectra). This predicted spectrum has been reduced in spectral resolution to match the ACE-FTS spectral response, and numerically apodized and resampled on the spectral grid defined by the ACE-FTS spectra. Next, the ACE-FTS raw average spectra are divided by the appropriate sections of the model spectrum. The resulting modified ACE spectra are shown in Fig. 1 (HgCdTe channel) and 2 (InSb channel), middle traces. All prominent solar features are removed, and the spectra are now dominated by the channel fringes, superimposed on the broadband spectral response.

We now take advantage of the fact that the channelling signal is comprised of a number of discrete, high-frequency, (quasi-) periodic oscillations, well separated

in the Fourier (interferogram) domain from the low-resolution contributions which comprise the spectral response of the measurement system. A smooth empirical response function is superimposed on the spectra as shown in Figs. 1 and 2. This response function has been constructed by applying a Gaussian filter of variable spread to take into account that the spectral response shows several localized absorption troughs. Dividing the spectra with the solar features removed by the smooth empirical response function reveals the channelling disturbances, which clearly dominate over the noise level (only near the edges of the two spectral bands does the noise contribute significantly as the response of the spectrometer falls off sharply).

A Fourier transform of this spectral pattern reveals the channelling periods as sharp spikes (Figs. 3 and 4). The final estimate for the pure channelling contribution is constructed by applying a sum of bandpass filters matched to the frequencies of the leading channelling contributions. The channel fringes are removed by ratioing the measured spectrum with this purified channelling modulation. The channelling frequencies are provided in Tables 1 (HgCdTe) and 2 (InSb). As can be seen from these figures and tables, the HgCdTe spectral band is much more difficult to clean than the InSb band, because numerous channelling frequencies are involved. Nevertheless, even in the HgCdTe band the spectrum can be improved significantly. In Fig. 5, a section of the ACE-FTS solar spectrum is shown before and after removing the channel

fringes to demonstrate how effective the applied cleaning procedure is. In the last step, the spectral response curve is applied, leaving us with the solar transmission spectrum obtained from the ACE measurements (Fig. 6).

It is important to note that the above procedure is not circular although a solar model spectrum has been used: the resulting ACE-FTS spectrum is not identical with the model transmission spectrum which has been introduced in the analysis. The model spectrum was used only to improve the detection limit for the channelling spikes in the Fourier domain by reducing the contribution of the solar features. The main defect in the constructed solar spectrum is that it has been high-pass filtered in the analysis process, so while individual solar lines are preserved, any broadband solar absorption features wider than several 10^5 cm^{-1} are removed and no information concerning the photospheric intensity as function of wavenumber is provided. To reflect these limitations we refer to this result as a “solar transmission spectrum” instead of a “solar spectrum”. The same caveat holds for the ATMOS solar spectrum as well, because on-orbit blackbody measurements are not available for ACE-FTS and ATMOS. Such auxiliary measurements would allow the actual broadband spectral sensitivities to be determined. Fig. 7 shows a section of the ACE-FTS solar transmission spectrum and the two ATMOS results. Due to the excellent noise level achieved in the ACE-FTS spectrum weak absorption features near 3030 cm^{-1} are clearly visible which are on the order of the noise level in the ATMOS ATLAS-3 spectrum.

Table 3

Description of the new assigned line list, giving number of lines, applied procedures, comments and some references for each species.

Species	Number of lines	References, procedures, comments
H	17	Garcia and Mack (1965) JOSA, 55, 654.
C I	130	Start with Geller, then use Wallace and Hinkle (2007) ApJS, 169, 159, and then use Chang and Geller (1998) Phys Scr, 58, 326 where W and H are of no help.
Na I	32	Start with Geller, insert lab frequencies and make a few corrections based on Martin and Zalubas (1981) J Phys Chem Ref Data 10, 153.
Mg I	158	Mostly Geller with insertions of lab frequencies from Kaufman and Martin (1991) J Phys Chem Ref Data 20, 83. Uncertainties persist here which seem to call for lab work in the IR.
Al I	48	Geller with lab frequencies from Kaufman and Martin (1991) J Phys Chem Ref Data 20, 775.
Si I	501	Ritz line positions from energy levels of Martin and Zalubas (1983) J Phys Chem Ref Data 12, 323 as extended by Geller. For the determination of the energy levels a number of solar lines have been included but with weight only 0.2. The total number of levels in the calculation was 165.
S I	28	Jakobsson (1966) Ark Fys 34, 19, Geller, and Martin, Zalubas and Muscrove (1990) J Phys Chem Ref Data 19, 821.
K I	15	Geller and Sugar and Corliss (1985) J Phys Chem Ref Data v14, Supplement no. 2.
Ca I	98	Geller and Sugar and Corliss (1979) J Phys Chem Ref Data 8, 865.
Ca II	7	As for Ca I.
Sc I	5	Geller lists three identifications and four tentative assignments for Sc in this region. Working mostly with Sugar and Corliss (1980) J Phys Chem Ref Data 9, 473, this is now worked down to two tentative assignments.
Ti I	16	Geller and Forsberg (1991) Phys Scr, 44, 446.
Cr I	26	Geller replaced by Wallace unpublished.
Fe I	958	Ritz wavenumbers from the energy levels of Nave et al. (1994) ApJS 94, 221, Nave et al. Phys Scr (1994) 49, 581, and Schoenfeld et al. (1995) Astron Astrophys, 301, 593.
Ni I	97	Geller, with wavenumbers changed to match Litzen, Brault and Thorne (1993) Phys Scr, 47, 628.
CO	8422	Frequencies from HITRAN, and ν and J limits on bands estimated from Geller. Many lines are blends.
OH	753	Melen et al. (1995) J Mol Spectrosc, 174, 490, for $\nu=0-3$ and Colin et al. (2002) J Mol Spectrosc, 214, 225 (from P. Bernath, priv. comm.) for $\nu=4$.
NH	57	Rotational lines from Geller et al. (1991) Astron Astrophys 249, 550, vib-rot lines from Grevesse et al. (1990) Astron Astrophys 232, 225, and extended with the Geller atlas.
CH	602	There is extensive background material for CH, lab work by Bernath (1987) J Chem Phys 86, 4838, and a much more extensive analysis of CH in the ATMOS spectra by Melen et al. (1989) J Mol Spectrosc 134, 305. What is used here is Geller's ATMOS atlas which is even more extensive than Melen et al.

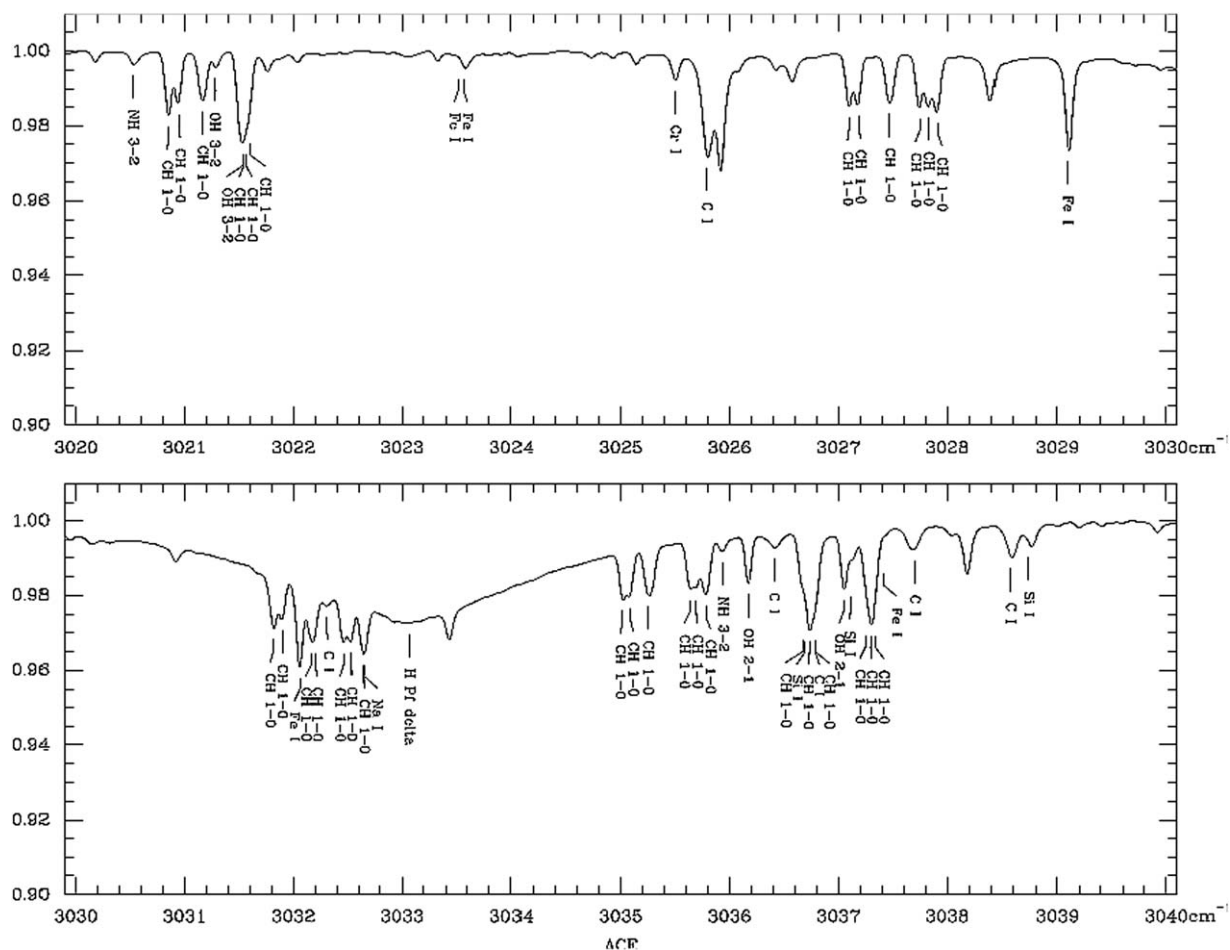


Fig. 8. A section of the ACE-FTS solar atlas with line assignments.

4. Description of the ACE-FTS solar atlas and line lists

Two line lists have been prepared for the ACE-FTS solar spectrum. The first of these is an observed line list, which was derived with the help of Carleer's WSpectra program [7]. This is a Windows program used to determine accurate line parameters from high resolution spectra. All spectral features were selected in the solar spectrum and their positions determined using a least-squares fit with Voigt lineshape functions. The line positions were then calibrated using rotational lines of the 1–0 fundamental band of OH, taken from the solar IR spectrum recorded by the ATMOS instrument [8]. It is difficult to find clean strong lines suitable for calibration in the dense solar spectrum and we estimate that our wavenumber calibration has an accuracy of $\pm 0.001 \text{ cm}^{-1}$.

The second line list is the list of wavenumbers and transitions applied to the atlas pages, based on the modified Geller line list [2]. This Geller line list was compared to the ACE-FTS solar spectrum and updated as appropriate. Laboratory or calculated Ritz values were used to show any disagreement between the lines in the spectrum and the best laboratory position that was found. Cr I and Si I were special cases for which Ritz values from unpublished energy

levels by Wallace have been used and included in the line list. Assignments were plotted on the ACE-FTS solar spectrum and final editing performed. Table 3 gives procedures, references and comments for each species.

The two line lists, the ACE-FTS solar atlas (in EPS and PDF formats), and the solar transmission spectrum (ASCII-table format) are all provided on the ACE homepage at the University of Waterloo (<http://www.ace.uwaterloo.ca/solaratlas.html>) and, except for the pdf and ps files, are also given in the electronic supplement to this paper. Fig. 8 shows a section of the ACE-FTS solar atlas including line assignments. To help in the assignment of the spectral signatures in the ACE solar spectrum with the line positions given in current spectroscopic line lists, a final empirical correction factor on the spectral abscissa of 1.00000294(26), equivalent to a shift of $+0.0088(8) \text{ cm}^{-1}$ at 3000 cm^{-1} was applied to the observed line list.

5. Conclusions and outlook

A new atlas of the infrared solar spectrum constructed from ACE-FTS observations has been presented. Due

to the excellent noise level achieved we have been able to assign numerous weak absorption features which were not detectable in the ATMOS solar observations.

A large number of dedicated high-sun spectra have been recorded with the ACE-FTS and are as yet unprocessed. For a future update, it is planned to also include this set of spectra along with the high sun spectra recorded for each occultation used in the present paper. In those spectral regions where the ACE-FTS sensitivity is high, the residual artefacts remaining after the channelling removal dominate over the noise level and the quality can hardly be improved. However, in regions of reduced sensitivity, especially at the upper end of the InSb band, the ACE-FTS solar spectrum could be further improved. In addition, more work is planned to further improve the current assigned line list, especially concerning the CH, NH, and OH absorbers. For example, an improved set of OH energy levels has just been published [9]. Future updates will be made available at <http://www.ace.uwaterloo.ca/solaratlas.html>.

Acknowledgments

The ACE mission is supported primarily by the Canadian Space Agency. JJH thanks the Natural Environment Research Council (NERC), UK, for financial support and some funding was also provided by the NASA laboratory astrophysics program. We thank J. Sauval for providing a copy of the updated ATMOS line assignments.

Appendix A. Supplementary material

Supplementary data associated with this article can be found in the online version at [doi:10.1016/j.jqsrt.2009.10.020](https://doi.org/10.1016/j.jqsrt.2009.10.020).

References

- [1] Farmer CB, Norton RH. A high resolution atlas of the Infrared spectrum of the sun and the earth atmosphere from space. vol. I. The Sun NASA Reference Publication 1224, Washington DC: National Aeronautics and Space Administration; 1989.
- [2] Geller M. A high resolution atlas of the infrared spectrum of the sun and the earth atmosphere from space. vol. III. Key to identification of solar features from 650 to 4800 cm^{-1} . NASA Reference Publication 1224, Washington, DC: National Aeronautics and Space Administration; 1992. Sauval AJ, Blomme R, Grevesse N, editors. Laboratory and astronomical high resolution spectra. In: ASP conference series; vol. 81. 1995. p. 88–101 (2400 identified lines) unpublished results, 1998 (2700 identified lines).
- [3] Abrams MC, Goldman A, Gunson MR, Rinsland CP, Zander R. Observations of the infrared solar spectrum from space by the ATMOS experiment. *Appl Opt* 1996;35:2747–51.
- [4] Bernath PF, McElroy CT, Abrams MC, Boone CD, Butler M, Camy-Peyret, C, et al. Atmospheric chemistry experiment (ACE): mission overview. *Geophys Res Lett* 2005;32:L15S01.
- [5] Abrams MC, Toon GC, Schindler RA. A practical example of the correction of Fourier transform spectra for detector nonlinearity. *Appl Opt* 1994;33:6307–14.
- [6] Hase F, Demoulin P, Sauval AJ, Toon GC, Bernath PF, Goldman, A, et al. An empirical line-by-line model for the infrared solar transmittance spectrum from 700 to 5000 cm^{-1} . *JQSRT* 1996;102:450–63.
- [7] Carleer MR. WSpectra: a Windows program to accurately measure the line intensities of high-resolution Fourier transform spectra. *Proc SPIE* 2001;4168:337. doi:10.1117/12.413851.
- [8] Mélen F, Sauval AJ, Grevesse N, Farmer CB, Servais CH, Delbouille, L, et al. A new analysis of the OH radical spectrum from solar infrared observations. *J Mol Spectrosc* 1995;174:490–509.
- [9] Bernath PF, Colin R. Revised molecular constants and term values for the $X^2\Pi$ and $B^2\Sigma^+$ states of OH. *J Mol Spectrosc* 2009;257:20–3.